Formation of quaternary all-d-metal Heusler alloy by Co doping fcc type Ni_2MnV and mechanical grinding induced B2–fcc transformation

Lu Peng(彭璐)[1], Qiangqiang Zhang(张强强)[1], Na Wang(王娜)[1], Zhonghao Xia(夏中昊)[1], Yajiu Zhang(张亚九)[2], Zhigang Wu(吴志刚)[2], Enke Liu(刘恩克)[3], and Zhuhong Liu(柳祝红)[1,†]

[1] *Department of Physics, University of Science and Technology Beijing, Beijing* 100083, *China*
[2] *School of Civil Engineering, Guangzhou University, Guangzhou* 510006, *China*
[3] *Beijing National Laboratory for Condensed Matter Physics, Institute of Physics, Chinese Academy of Sciences, Beijing* 100190, *China*

(Received 1 January 2022; revised manuscript received 12 March 2022; accepted manuscript online 17 March 2022)

The structure of the all-d-metal alloy $Ni_{50-x}Co_xMn_{25}V_{25}$ ($x = 0$–50) is investigated by using theoretical and experimental methods. The first-principles calculations indicate that the most stable structure of the Ni_2MnV alloy is face-centered cubic (fcc) type structure with ferrimagnetic state and the equilibrium lattice constant is 3.60 Å, which is in agreement with the experimental result. It is remarkable that replacing partial Ni with Co can turn the alloy from the fcc structure to the B2-type Heusler structure as Co content $x > 37$ by using the melting spinning method, implying that the d–d hybridization between Co/Mn elements and low-valent elements V stabilizes the Heusler structure. The Curie temperature T_C of all-d-metal Heuser alloy $Ni_{50-x}Co_xMn_{25}V_{25}$ ($x > 37$) increases almost linearly with the increase of Co due to that the interaction of Co–Mn is stronger than that of Ni–Mn. A magnetic transition from ferromagnetic state to weak magnetic state accompanying with grinding stress induced transformation from B2 to the dual-phase of B2 and fcc has been observed in these all-d-metal Heusler alloys. This phase transformation and magnetic change provide a guide to overcome the brittleness and make the all-d-metal Heusler alloy interesting in stress and magnetic driving structural transition.

Keywords: all-d-metal Heusler alloy, grinding induced phase transformation, phase stability

PACS: 71.20.Be, 71.20.Lp, 61.05.cp **DOI:** 10.1088/1674-1056/ac5e94

1. Introduction

The Heusler alloy is a large family of functional materials exhibiting different properties, including half-metallicity,[1,2] Hall effect,[3,4] magnetoresistance,[5] shape memory effect,[6] magnetocaloric effect (MCE),[7] and Weyl semimetal.[8–11] The conventional Heusler alloy has a cubic $L2_1$ structure consisting of four face-centered cubic sublattices with the formula X_2YZ, where X, Y are transition d metals, and Z is a main group element. The positions of four face-centered cubic sublattices are A (0, 0, 0), B (0.25, 0.25, 0.25), C (0.5, 0.5, 0.5), and D (0.75, 0.75, 0.75). It has been suggested that the p–d hybridization between the main group element and its nearest neighboring transition metals can stabilize the Heusler phase.[12,13] Therefore, the main group element is considered to be an essential element for the Heusler alloy.

All-d-metal Heusler alloy, as the name implies, all elements that compose the alloy are transition metal elements. This concept was first proposed by Liu *et al.* in 2015.[14] They reported that all-d-metal alloys $Ni_{50}Mn_{50-x}Ti_x$, $Mn_{50}Ni_{50-x}Ti_x$, and Ni–Mn–Co–Ti crystalized in the Heusler structure and exhibited martensitic transformation. They proposed that the physical mechanism of phase formation for the all-d-metal Heulser alloys is the d–d covalent hybridization, which has the same effect as the p–d hybridization in the conventional Heusler alloy, playing a crucial role in the stability of the Heusler structure. Subsequently, they reported the electronic behavior of another all-d-metal Heusler shape memory alloy $Ni_{50-x}Fe_xMn_{35}Ti_{15}$[15] during martensitic transformations (MT), and proposed a spintronic property based on the magnetic structure phase transition.

Strictly speaking, Heusler alloys usually have a highly ordered $L2_1$ structure. However, the disorder between B and D sites as well as other sites in Heusler alloys is a very common phenomenon in practice, such as Co_2MnSi and Ni_2MnGa.[16,17] In this case, it is usually called the B2-type Heusler alloy.[18] The (dis)ordering behaviors and their effects on the physical properties of Heusler alloys have been widely studied.[19,20] Compared with the conventional Heusler alloys, all-d-metal Heusler alloys are more easily to form the B2-type or more ordered $L2_1$-type Heusler structure, i.e., $Ni_{50}Mn_{50-x}Ti_x$, Fe_2CrV–Cr_2FeV, and Co_2MnTi.[14,21,22] As a new family of Heusler alloys, all-d-metal Heusler alloys bear a great advantage of high toughness, which is more important for practical engineering applications of functional Heusler alloys.[23–25] However, from the view of the chemical bonding, the covalent bonding ability between d–d is weaker than that of between p–d, so it is not easy to form the Heusler structure if X, Y, and Z are all transition metals. For exam-

†Corresponding author. E-mail: zhliu@ustb.edu.cn

© 2023 Chinese Physical Society and IOP Publishing Ltd

ple, as Cr content $x \geq 0.5$, $Mn_2NiGa_{1-x}Cr_x$ alloys transform from the Heusler structure to the pure face-centered cubic (fcc) phase.[26] This implies that the all-d-metal alloys may exhibit multiphase competition upon phase formation, i.e., fcc-type disordered γ phase, fcc-type ordered $L1_2$ structure, and B2-type phase.

The structure and the phase of the materials impose significant influence on the functional properties. For example, the hexagonal $MnNi_{0.77}Fe_{0.23}Ge$ alloy can effectively change the magnetic structural transition temperature of this system by applying hydrostatic pressure, thus changing the associated MCE.[27] The tetragonal Heusler alloy Mn_3Ga presents a large coercive field of 359 kA/m with saturation magnetic moment of $1.1\mu_B$ at 5 K,[28] having the potential application for spin-transfer torque (STT) device, while fcc Mn_3Ga alloy shows a typical antiferromagnetic nature.[29] In Heusler alloys with martensitic transformation, the mechanical property of the alloys can be enhanced by the presence of a little amount of γ phase. However, the martensitic transformation will be suppressed due to the large fraction of the γ phase. Furthermore, the investigation of the functional properties of the alloys subjected to various deformation is important for practical applications.[30] So the mechanical properties of the Heusler alloys have also attracted much interest. In the Fe–Mn–Al[31] and Fe–Mn–Ga[32] alloys, stress induced B2 $\rightarrow \gamma$ phase transformation has been observed, making them have good cold deformation ability. In this regard, it is essential to investigate the formation and mechanical deformation of the all-d-metal Heusler phase.

First-principles calculations have predicted that the hypothesis all-d-metal Heusler alloy Ni_2MnV has martensitic transformation.[33,34] However, our experiment finds that it is difficult to crystalize in Heusler structure for Ni_2MnV. It has been reported that Co_2VMn has B2 structure with a Curie temperature (T_C) of 670 K and a saturation magnetization of 145.1 emu/g.[35] It seems promising that using Co substitution partial Ni in Ni_2MnV can stabilize the body-centered cubic (bcc) structure. So Co doping partial Ni in Ni_2MnV is adopted in this research.

All-d-metal alloys $Ni_{50-x}Co_xMn_{25}V_{25}$ (x = 0–50) are prepared in this study. It has been found that the pure Heusler phase formed by melt-spinning method as Co content $x >$ 37, indicating that the d–d covalent bonding effect between Co/Mn and V atoms facilitates the B2-type Heusler phase formation. However, the γ phase has been observed embedded in the β matrix in the as-melted ingot in samples of $x >$ 37. The fraction of γ phase gradually decreases with the increase of Co content. Furthermore, a grinding stress induced phase transformation from B2 to the mixture of B2 and fcc γ phase is observed. Accompanying with this structural transition, a magnetic change from ferromagnetic to weak magnetism occurs, suggesting the potential for multi-field–driven application.

2. Experiment and method

$Ni_{50-x}Co_xMn_{25}V_{25}$ (x = 0–50) ingots were prepared by arc-melting the high purity (99.99% or higher) Ni, Co, Mn, and V elements. The ingots were remelted at least four times for homogenization. Part of the ingots was subsequently melted in a quartz tube and rapidly cooled by spinning onto the surface of a copper wheel, spinning at a linear velocity of about 25 m/s. X-ray diffraction (XRD) patterns were recorded by the Rigaku Smartlab3 instrument with Cu $K\alpha$ radiation to characterize the crystal structure. The step size of 0.02° and three seconds step time were adopted during the measurement. Differential scanning calorimetry (NETZSCH, DSC 214 Polyma) curves were obtained with a heating/cooling rate of 10 K/min to determine the characteristic temperatures of phase transformation and Curie transition. Magnetic properties were measured by superconducting quantum interference device (SQUID) magnetometer.

The electronic structures are calculated by using the Vienna *ab initio* simulation package (VASP) with the projector-augmented wave (PAW) scheme based on the density functional theory (DFT).[36] The electronic exchange–correlation function is described by the generalized gradient approximation of Pardew, Burke, and Ernzerhof (GGA-PBE).[37,38] For Ni_2MnV, ordered $L2_1$-type (Cu_2MnAl-type with space group $Fm3m$, No. 225), XA-type (Hg_2CuTi-type with space group $F\bar{4}3m$, No. 216), and fcc-type (CuAu-type with space group $P4/mmm$, No. 123) structures (see Fig. 1) are calculated to find the stabilization of the alloy. Furthermore, different magnetic configurations including ferrimagnetic (FIM), ferromagnetic (FM), and non-magnetic (NM) are also taken into consideration, where FIM indicates spins between the Mn and V atoms are anti-parallel, and the parallel case is FM. The cut-off energy of 500 eV and a self-consistent field of 10^{-7} eV are used to achieve good convergence.

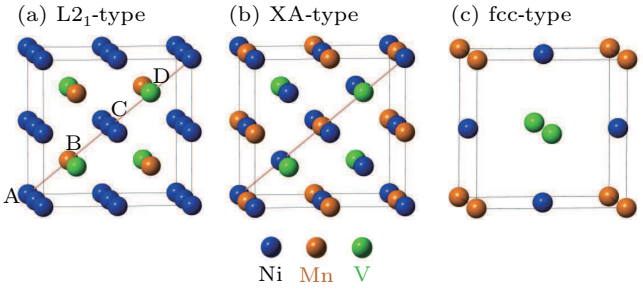


Fig. 1. The schematic cells of ordered $L2_1$-type (a) XA-type (b) Heusler structures, and (c) fcc (123 space group) structure.

3. Results and discussion

Figure 2(a) shows the calculated total energy of Ni_2MnV as a function of volume for different crystal structures (or-

dered $L2_1$-type, XA-type Heusler structures, and fcc structure) and different magnetic configurations (FIM, FM, and NM). It is noted that the magnetic configurations of XA and fcc structures eventually converge to FIM whether the magnetic configuration is FM or FIM. This implies that magnetic configuration of FM cannot exist stably in XA and fcc structures. Therefore, only FIM/NM states are given in Fig. 2(a) for both XA and fcc structures. It can be found that the XA-type FIM structure has lower energy than that of the $L2_1$-type FIM structure, and the minimum energy difference between the two states is 0.50 eV/cell. The total energy of the fcc-type structure with FIM coupling is the lowest, which indicates that Ni_2MnV is more inclined to form a FIM fcc structure. The calculated equilibrium lattice constant for the FIM fcc-type alloy is $a = 3.60$ Å. Figure 2(b) shows the XRD pattern for the Ni_2MnV ribbon sample. The characteristic peaks can be indexed to fcc structure with the lattice parameter of $a = 3.63$ Å, and they are consistent with the theoretical calculation.

The total density of states (TDOS) and partial density of states (PDOS) of d electrons for XA-type and fcc-type Ni_2MnV (FIM state) are shown in Figs. 2(c) and 2(d). For the TDOS of the XA-type alloy (see Fig. 2(c)), the Fermi energy (E_F) falls into a pseudo-energy gap in the spin-up direction. However, E_F situates in a relatively high narrow peak of 3d states in the minority spin direction of the TDOS curve, showing a high spin polarization of the alloy. This peak is mainly attributed to 3d electrons of Ni, Mn, and V, implying the strong d–d hybridization between them. The TDOS of the fcc Ni_2MnV (see Fig. 2(d)) is different from that of the XA-type structure. For the spin-up direction, E_F shifts to the left side of the pseudo-energy gap, having 2.172 states/eV per spin, while E_F falls into a TDOS valley in the spin down direction, having 7.805 states/eV per spin. The degree of spin polarization of the charge carriers at E_F is only 56.5%. It is generally considered that if E_F situates at the peak of TDOS, the structure is unstable. This is called the DOS criterion to determine which structure is more stable.[39] Together with the energy–volume curve, it can be concluded that the fcc structure is more stable than XA-type Heusler structure for Ni_2MnV as a consequence of the TDOS behavior.

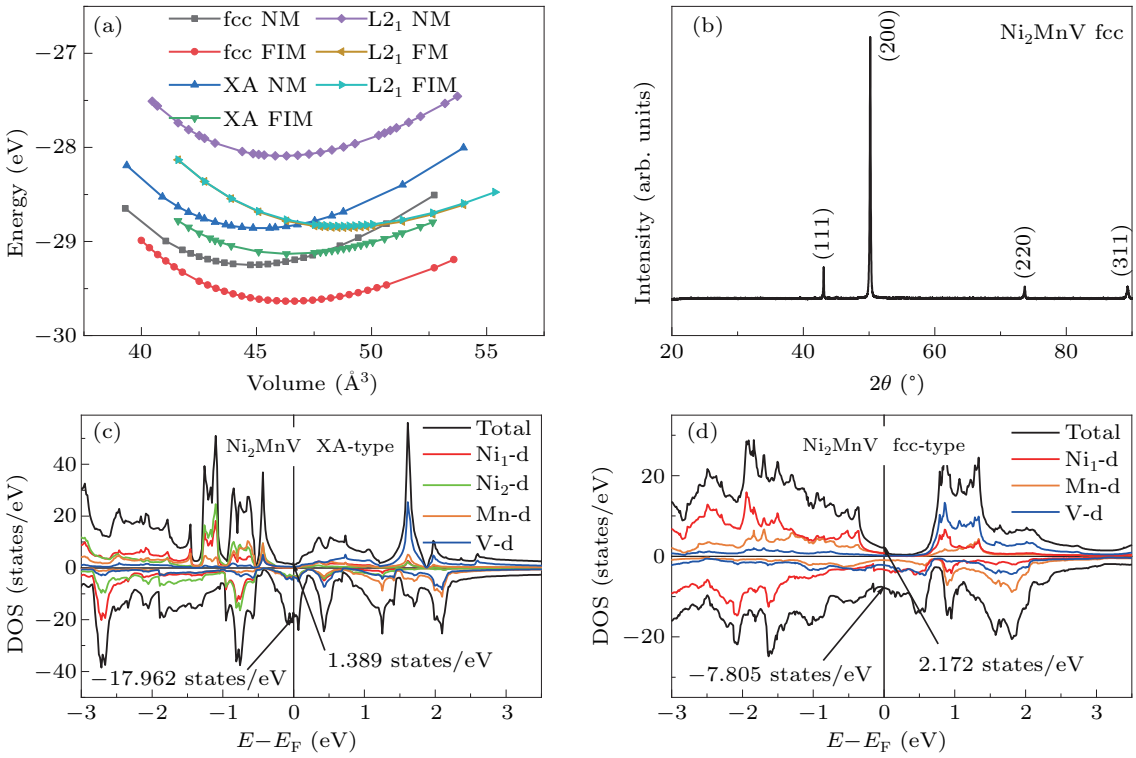


Fig. 2. (a) The total energies as a function of volume for Ni_2MnV alloy with ordered $L2_1$-type, cubic XA-type, and fcc structures in ferromagnetic (FM), ferrimagnetic (FIM), and non-magnetic (NM) states. (b) XRD pattern for Ni_2MnV ribbon measured at room temperature. Calculated TDOS and PDOS of d electrons for Ni_2MnV with cubic XA-type (c), and fcc (123 space group) (d) FIM structures.

Previous report has confirmed that Co_2VMn has bcc structure.[35] It seems that Co can enhance the stabilization of Heusler structure. So, the element Co is selected to substitute partial Ni in the Ni_2MnV. Figures 3(a)–3(c) show the XRD patterns of $Ni_{50-x}Co_xMn_{25}V_{25}$ ($x = 0$–50) melt-spun ribbons measured at room temperature. The plot shows that the pure fcc phase of Ni_2MnV is kept when $0 < x < 30$. The lattice parameter of fcc phase decreases with the increase of Co, as listed in Table 1. Extra peaks start to appear except for the main peaks of the fcc structure when x increases to 30. The extra peaks can be indexed to the $Co_{1.9}V_{3.1}$-type tetragonal phase (space group $P42/mnm$).[40] We use the symbol T before the Miller indices to identify the peaks of the tetragonal structure. This tetragonal phase is different from the tetrag-

onal Heusler structure, which has a space group *I*4/*mmm* or $I\bar{4}m2$.[41] The ratio of $Co_{1.9}V_{3.1}$-type tetragonal phase in the XRD pattern for $x = 32$ increases compared with $x = 30$. Further increasing x to 34, except for the tetragonal phase, the peak intensity of fcc weakens greatly and the peaks of the bcc structure appear. Both lattice parameters of a and c for the tetragonal phase decrease with an increase of x from 30 to 34 (see Table 1). The lattice parameter of fcc phase from $x = 30$ to $x = 34$ also decreases gradually. Overall, the lattice parameter for the fcc phase decreases with the increase of Co content. For $x = 37$, the bcc phase dominates the structure of the alloy.

As $x > 37$, the phase can be determined as a pure bcc phase (see Fig. 3(c)), which has the same structure as observed in all-d-metal Heusler alloys Ni–Mn–Ti, Fe_2CrV, NiMnTi, NiCoMnTi, and Co_2MnTi.[14,21,22,42] Since the lack of (111) superlattice peak, and only (200) superlattice peak can be observed, it is suggested that disorder formed between sites B and D, namely Mn and V, confirming the formation of B2-type Heusler phase.[14,21,22,43] It is proposed that the d–d covalent hybridization effect between the nearest neighboring 3d transition metals can stabilize the Heusler structure, such as the d–d covalent bonding between Ni/Mn and Ti can promote the formation of the Heusler phase of Ni_2MnTi.[44] The phase of $Ni_{50-x}Co_xMn_{25}V_{25}$ changes to the Heusler phase as $x > 37$, which suggests that the d–d covalent bonding between Co–Mn and Co–V atoms is stronger than that between Ni–Mn and Ni–V, helping to stabilize the B2-type Heusler phase.

The lattice parameters for all-d-metal Heusler alloys $Ni_{50-x}Co_xMn_{25}V_{25}$ (x = 0–50) are calculated according to XRD, as shown in Table 1. It can be found that a decreases with the increase of Co content, changing from 5.8198 Å in $x = 37$ to 5.8000 Å in $x = 50$. As the increase of Co, the distances between Co–Mn and Co–V decrease, resulting in the enhancement of d–d covalent bonding.

Table 1. The lattice parameters of fcc, $Co_{1.9}V_{3.1}$-type tetragonal and B2-type Heusler phases in $Ni_{50-x}Co_xMn_{25}V_{25}$ (x = 0–50) ribbons.

Ribbon Co (x)	fcc a (Å)	Ribbon Co (x)	Tetrgonal a (Å)	c (Å)	fcc a (Å)	B2 a (Å)	Ribbon Co (x)	B2 a (Å)
$x = 0$	3.6336	$x = 30$	8.8585	4.6056	3.6233	–	$x = 38$	5.8181
$x = 5$	3.6352	$x = 32$	8.8534	4.5959	3.6221	–	$x = 40$	5.8170
$x = 10$	3.6279	$x = 34$	8.8480	4.5921	3.6206	5.8282	$x = 45$	5.8087
$x = 15$	3.6258	$x = 35$	8.8398	4.5852	3.6198	5.8221	$x = 47$	5.8032
$x = 20$	3.6253	$x = 37$	–	–	–	5.8198	$x = 50$	5.8000
$x = 25$	3.6257	–	–	–	–	–	–	–

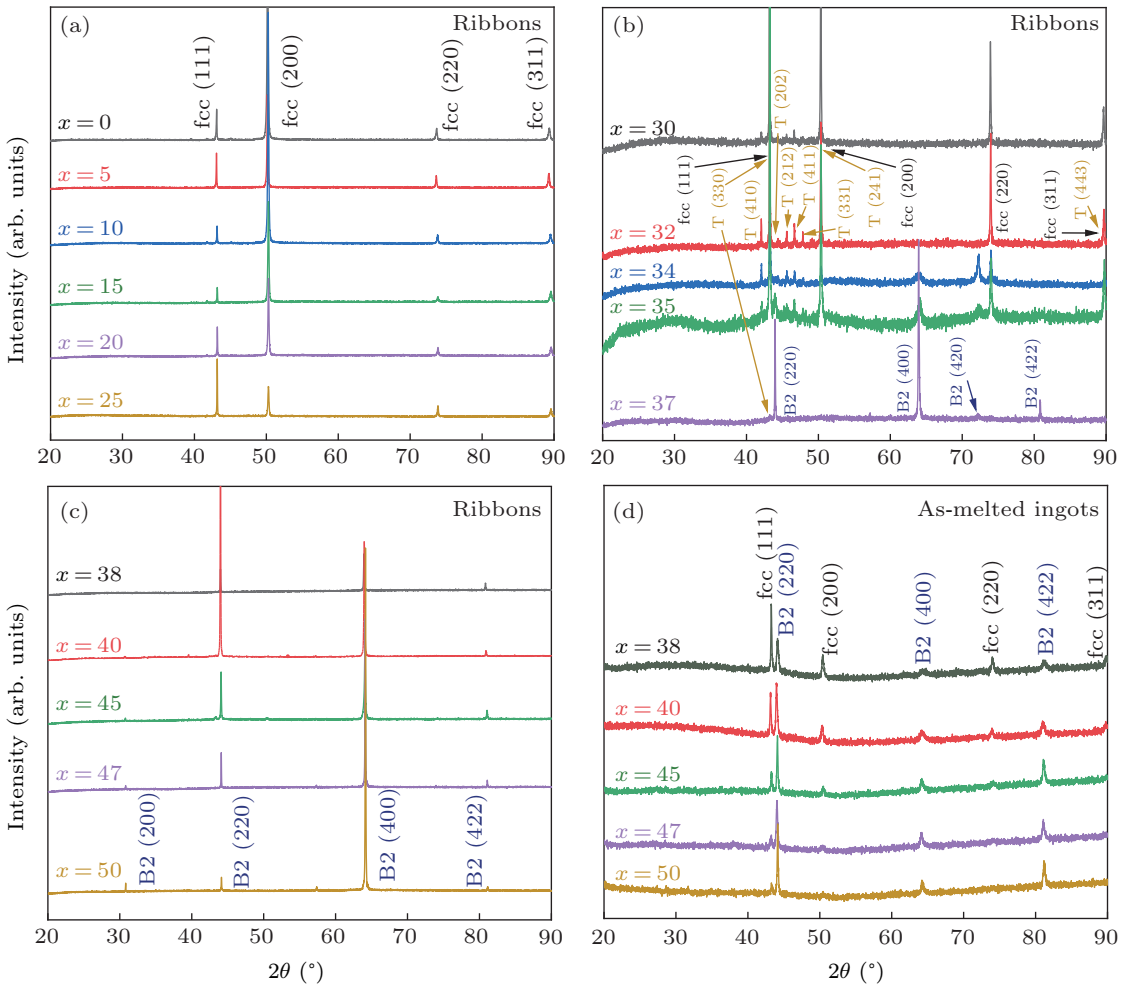


Fig. 3. (a)–(c) XRD patterns of $Ni_{50-x}Co_xMn_{25}V_{25}$ (x = 0–50) ribbons measured at room temperature. (d) XRD patterns of $Ni_{50-x}Co_xMn_{25}V_{25}$ ($x > 37$) as-melted ingots measured at room temperature.

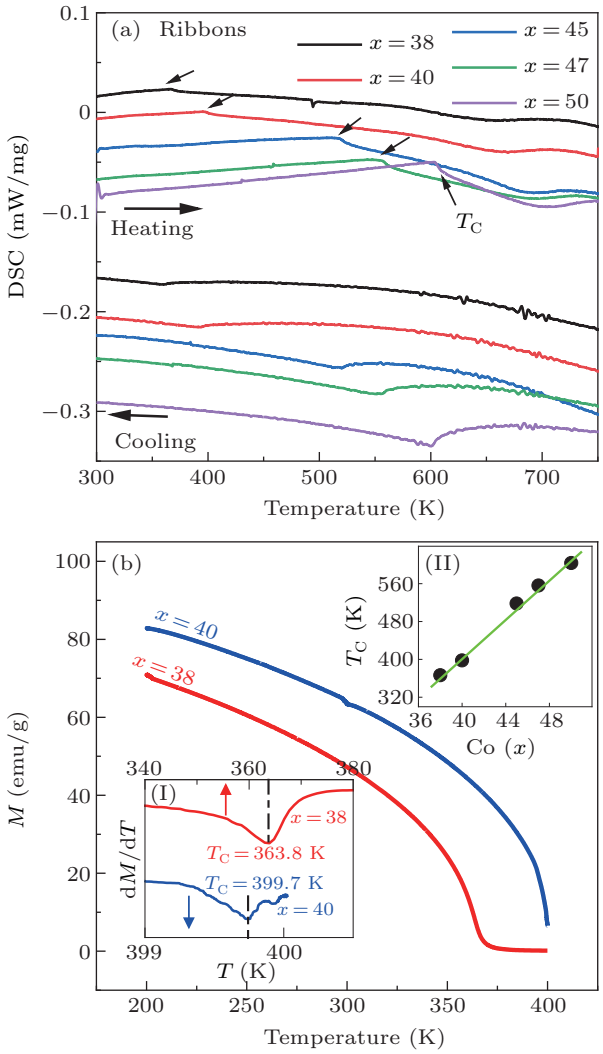


Fig. 4. (a) The DSC curves for $Ni_{50-x}Co_xMn_{25}V_{25}$ ($x = 38$, 40, 45, 47, 50) ribbons. (b) The temperature dependence of magnetization $M(T)$ of $Ni_{50-x}Co_xMn_{25}V_{25}$ ($x = 38$, 40) ribbons measured at 100 Oe field. Inset (I) shows the dM/dT versus T measurements to calculate the Curie temperatures. Inset (II) shows T_C as a function of Co content x.

To study the phase formation of all-d-metal alloy $Ni_{50-x}Co_xMn_{25}V_{25}$ ($x > 37$) ribbons with pure Heusler structure, the XRD spectrum of the as-melted ingots for $x > 37$ is also investigated. The ingots are cut into slice and then directly measured the patterns at room temperature. Compared with the ribbon samples, the as-melted ingots are no longer pure Heusler phase. Mixed phases of fcc and B2 appeared, as shown in Fig. 3(d). Furthermore, the peaks of the fcc phase weaken gradually and the Heusler phase plays the dominant role with the increase of Co. There is only a rather small (111) peak of the fcc structure in Co_2MnV. This also suggests that Co can help to stabilize the Heusler structure. The solidification rate in melt-spinning process is more rapid than that in arc-furnace melting process, thus it can avoid low temperature phase region and directly forms the high temperature phase, which impedes the formation of the fcc phase.

We perform DSC measurements on the ribbon samples through a heating and cooling process in the temperature range from 150 K to 873 K for $Ni_{50-x}Co_xMn_{25}V_{25}$ ($x > 37$) ribbons with pure Heusler structure. No phase transition is detected below room temperature, so we only give the curves from 300 K to 800 K, as shown in Fig. 4(a). A small endothermic transformation peak upon heating and an exothermic peak during cooling process occurring nearly at the same temperature can be observed, suggesting that the peak temperature is probably corresponding to the Curie transition of the alloy. In order to exclude whether these weak peaks are caused by order–disorder transformation, the thermomagnetization (M–T) curves for $Ni_{50-x}Co_xMn_{25}V_{25}$ ($x = 38$, 40) ribbons under 100 Oe magnetic field are measured, as shown in Fig. 4(b). It is obvious that both samples show a second-order Curie transition. The temperature dependence of dM/dT is shown in inset (I) of Fig. 4(b). From the peak temperature of the derivative curve of $M(T)$, T_C are determined to be 363.8 K and 399.7 K for $x = 38$ and 40, respectively, which is consistent with the peak temperature of the DSC curves. This confirms that the weak peak temperature is indeed T_C. Inset (II) shows the T_C as a function of x. It can be found that T_C increases from 366.4 K for $x = 38$ to 603.5 K for $x = 50$, almost linearly with Co content with the slope of 19.8 K per Co atom. In the $Ni_{50-x}Co_xMn_{25}V_{25}$ alloy, the Mn–Mn, Ni–Mn, and Co–Mn interactions dominate the Curie transition. The interaction between the nearest neighboring Co–Mn is usually stronger than that between Ni–Mn. More Co–Mn interaction is introduced by using Co atoms doping Ni atoms. The fraction of Co–Mn increases and Ni–Mn decreases, resulting in the increase of T_C. The T_C of our Co_2VMn ribbon is lower than 670 K. The T_C of bulk material Co_2VMn is reported by Ruan *et al.*[35] This may be attributed to different preparation method and small composition difference.

To test the mechanical deformation stability of all-d-metal Heuser alloy $Ni_{50-x}Co_xMn_{25}V_{25}$ ($x > 37$) ribbons, they are ground into powders. It should be noted that the all-d-metal Heuser alloy $Ni_{50-x}Co_xMn_{25}V_{25}$ ($x > 37$) ribbons transform from the pure Heusler phase to the mixed phases of fcc and B2 when the ribbons are ground into powders, as shown in Fig. 5. During the grinding process, it is found that the ribbons can only be ground into small pieces and are difficult to form fine powders, showing good ductility. This suggests that the induced fcc phase is ductile γ phase. It is clear that there is a grinding stress induced phase transformation in $Ni_{50-x}Co_xMn_{25}V_{25}$ ($x > 37$) ribbons with B2-type Heusler structure, indicating that the B2-type phase is a metastable phase. The single high temperature phase of B2 can be retained by fast cooling. While the melted ingot sample is mixed phases of B2 and fcc γ, as shown in Fig. 3(d). This implies that the γ phase should be the low temperature phase compared with B2. When the stress is applied, a B2–γ phase transformation is induced. Similar behavior has been observed in

the conventional Heusler alloy Fe–Mn–Al.[31] They attribute this behavior to the stress-induced martensitic transformation. Our discovery indicates that all-d-metal Heusler alloys have the great potential of achieving cold-deformation.

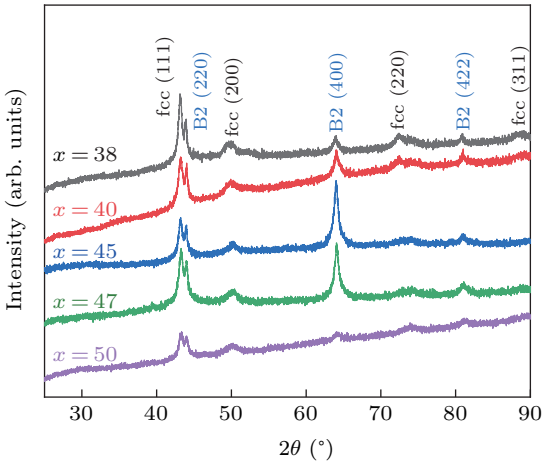


Fig. 5. Room temperature XRD patterns for $Ni_{50-x}Co_xMn_{25}V_{25}$ ($x > 37$) ribbons after grinding into small pieces.

The schematic phase diagram for $Ni_{50-x}Co_xMn_{25}V_{25}$ is given in Fig. 6. The phase formation of the all-d-metal Heusler alloy for Co doping fcc Ni_2MnV can be summarized. The B2-type Heusler phase starts to appear when $x > 34$ in both ribbons and as-melted ingots (see supplementary material), but the pure B2 phase is only formed in alloy with $x > 37$ by melt-spinning method. The grinding stress can induce partial B2 → fcc phase transformation.

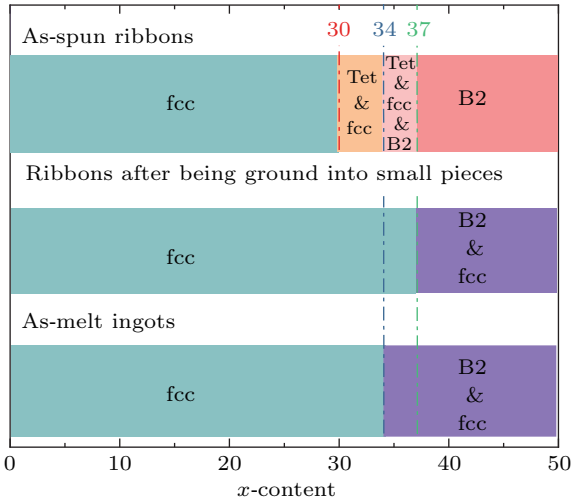


Fig. 6. Schematic structural phase diagrams of experimental (We use the abbreviation Tet to identify the tetragonal structure).

Figure 7 shows the initial magnetization curves at 5 K for all-d-metal Heuser alloy $Ni_{50-x}Co_xMn_{25}V_{25}$ ($x > 37$) as-spun ribbons and as-ground ribbon pieces. For both series samples, the saturation magnetization increases as Co content increases to $x = 47$ and then decreases when increasing Co content x to 50. It is worth noting that the spontaneous moment decreased greatly in as-ground samples, which is about 4.65 μ_B/f.u. for $x = 38$ ribbon, decreased to 2.25 μ_B/f.u. for the as-ground sample with a reduction rate of 50% (see the inset of Fig. 7(a)). This demonstrates the presence of magnetic change from ferromagnetism to weak magnetism accompanied by the structural phase transition. At the same time, it is harder to achieve saturation in as-ground sample compared with as-spun ribbons, which should attribute to the appearance of the fcc phase and the internal stress caused by grinding.

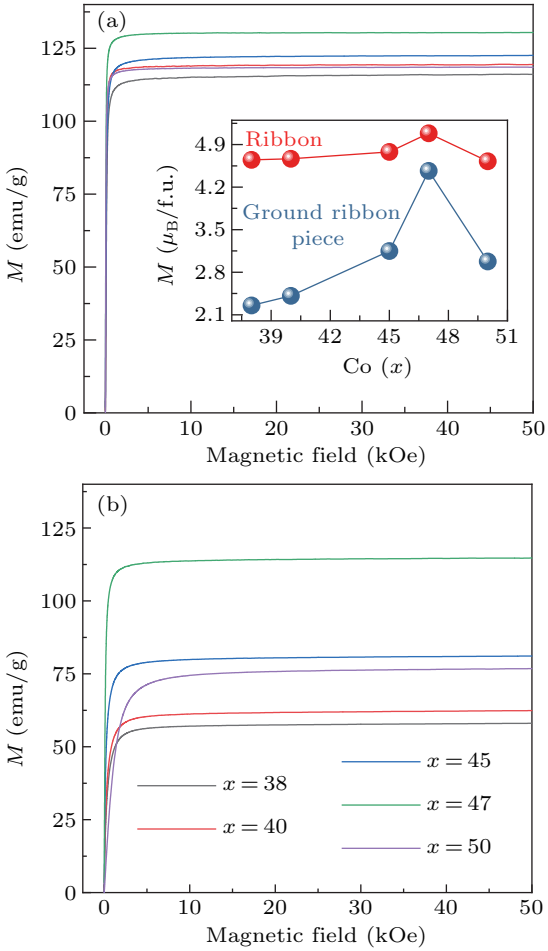


Fig. 7. Magnetization curves of $Ni_{50-x}Co_xMn_{25}V_{25}$ ($x > 37$) as-spun ribbons (a) and as-ground ribbon pieces (b) measured at 5 K in magnetic fields up to 5 T. The inset plot shows the variation of saturation magnetic moment with Co content x.

4. Conclusion

First-principles calculations indicate that the Ni_2MnV alloy prefers to crystalize in the FIM fcc-type structure with the equilibrium lattice constant of 3.60 Å, consisting with the experimental result. The lower DOS of the fcc state near the Fermi level can explain the stability of the fcc phase of Ni_2MnV. The structure of Co doping Ni in fcc Ni_2MnV is investigated simultaneously. It is demonstrated that pure Heusler phase is formed as Co content $x > 37$, indicating that the d–d hybridization between Co/Mn elements and low-valent elements V stabilizes the Heusler phase. However, the as-melted ingot samples $Ni_{50-x}Co_xMn_{25}V_{25}$ ($x > 37$) show

dual phase with fcc and B2. Furthermore, the pure Heusler alloy $Ni_{50-x}Co_xMn_{25}V_{25}$ ($x > 37$) is very sensitive to the stress. Grinding stress induced Heuser phase to dual-phase of fcc and B2 is observed in these all-d-metal Heusler alloys. Accompanying with this phase transition, a ferromagnetism to weak magnetism has been detected. These behaviors provide insight into the recently proposed all-d-metal Heusler alloys dominated by d–d covalent hybridization.

Acknowledgments

Project supported by the National Natural Science Foundation of China (Grant Nos. 51671024 and 52088101), State Key Lab of Advanced Metals and Materials (Grant No. 2019-Z12), and the Fundamental Research Funds for the Central Universities (Grant No. FRF-BD-20-12A).

References

[1] de Groot R A, Mueller F M, van Engen P G and Buschow K H J 1983 *Phys. Rev. Lett.* **50** 2024
[2] Balke B, Fecher G H, Kandpal H C, Felser C, Kobayashi K, Ikenaga E, Kim J J and Ueda S 2006 *Phys. Rev. B* **74** 104405
[3] Chen C, Wang H Q, Yang Z L and Zhang H J 2021 *Chin. Phys. Lett.* **38** 057302
[4] Wang Q, Du Q H, Petrovic C and Lei H C 2020 *Chin. Phys. Lett.* **37** 027502
[5] Sakuraba Y, Izumi K, Iwase T, Bosu S, Saito K and Takanashi K 2010 *Phys. Rev. B* **82** 094444
[6] Zhang X, Cui T Y, Liu Q S, Dong Z Z and Man C 2021 *J. Alloys Compd.* **858** 157685
[7] Liu Y F, Zhang X X, Xing D W, Shen H X, Chen D M, Liu J S and Sun J F 2014 *J. Alloys Compd.* **616** 184
[8] Hirschberger M, Kushwaha S, Wang Z J, Gibson Q, Liang S H, Belvin C A, Berneving B A, Cava R G and Ong N P 2016 *Nat. Mater.* **15** 1161
[9] Dulal R P, Dahal B R, Forbes A, Bhattari N, Pegg L and Philip J 2019 *Sci. Rep.* **9** 3342
[10] Swekis P, Sukhanov A S, Chen Y C, Gloskovskii A, Fecher G H, Panagiotopoulos I, Sichelschmidt J, Ukleev V, Devishvili A, Vorobiev A, Inosov D S, Goennenwein S T B, Felser C and Markou A 2021 *Nanomaterials* **11** 251
[11] Leiva L, Granville S, Zhang Y, Dushenko S, Shigematsu E, Shinjo T, Ohshima R, Ando Y and ShiraishiLeiva M 2021 *Phys. Rev. B* **103** L041114
[12] Niculescu V, Burch T J, Rag K and Budnick J I 1977 *J. Magn. Magn. Mater.* **5** 60
[13] Gelatt C D, Williams A R and Moruzzi V L 1983 *Phys. Rev. B* **27** 2005
[14] Wei Z Y, Liu E K, Chen J H, Li Y, Liu G D, Luo H Z, Xi X K, Zhang H W, Wang W H and Wu G H 2015 *Appl. Phys. Lett.* **107** 022406
[15] Zeng Q Q, Shen J L, Zhang H N, Chen J, Ding B, Xi X K, Liu E K, Wang W H and Wu G H 2019 *J. Phys.: Condens. Mat.* **31** 425401
[16] Abdallah I, Pradines B, Ratel-Ramond N, BenAssayag G, Arras R, Calmels L, Bobo J F, Snoeck E and Biziere N 2017 *J. Phys. D: Appl. Phys.* **50** 035003
[17] Vargova Z, Ryba T, Ilkovic S, Reiffers M, Komanicky V, Gyepes R and Varga R 2015 *J. Electr. Eng.* **66** 98
[18] Yuhasz W M, Schlagel D L, Xing Q, McCallum R W and Lograsso T A 2010 *J. Alloys Compd.* **492** 681
[19] Kudryavtsev Y V, Oksenenko V A, Lee N N, Lee Y P, Rhee J Y and Dubowik J 2005 *J. Appl. Phys.* **97** 113903
[20] Oksenenkoa V A, Kulagina V A, Kudryavtseva Y V, Dubowikb J, Gos´cian´skac I and Troshchenkov Y N 2007 *J. Magn. Magn. Mater.* **316** e407
[21] Shen J L, Zeng Q Q, Zhang H G, Xia X K, Liu E K and Wu G H 2019 *J. Magn. Magn. Mater.* **492** 165661
[22] Sanvito S, Oses C, Xue J K, Tiwari A, Zic M, Archer T, Tozman P, Venkatesan M, Coey M and Curtarolo S 2017 *Sci. Adv.* **3** e1602241
[23] de Paula V G, de Oliveira L S, Mendes Filho A A, Rios C T and Souza J A 2020 *J. Mater. Res.* **35** 3004
[24] Yan H L, Wang L D, Liu H X, Huang X X, Jia N, Li Z B, Yang B, Zhang Y D, Esling C, Zhao X and Zuo L 2019 *Mater. Des.* **184** 108180
[25] de Paula V G and Reis M S 2021 *Chem. Mater.* **33** 5483
[26] Sun K C, Shi X Y, Gao R R and Luo H Z 2021 *J. Phys. Chem. Solids* **157** 110204
[27] Zeng Q Q, Shen J L, Liu E K, Xue K X, Wang W H, Wu G H and Xi X Z 2020 *Chin. Phys. Lett.* **37** 076101
[28] Balke B, Fecher G H, Winterlik J and Felser C 2007 *Appl. Phys. Lett.* **90** 152504
[29] Kharel P, Huh Y, Al-Aqtash N, Shah V R, Sabirianov R F, Skomski R and Sellmyer D J 2014 *J. Phys.: Condens. Mat.* **26** 126001
[30] Guo J P, Zhong M T, Zhou W, Zhang Y J, Wu Z G, Li Y C, Zhang J S, Liu Y N and Yang H 2021 *Mater.* **14** 2339
[31] Walnsch A, Kriegel M J, Motylenko M, Korpala G, Prahl U and Leineweber A 2021 *Scr. Mater.* **192** 26
[32] Zhang Y J, Wu Z G, Hou Z P, Liu Z H, Liu E K, Xi X K, Wang W H and Wu G H 2021 *Appl. Phys. Lett.* **119** 142402
[33] Han Y L, Wu M X, Feng Y, Cheng Z X, Lin T T, Yang T, Khenata R and Wang X T 2019 *IUCrJ* **6** 465
[34] Tan J G, Liu Z H, Zhang Y J, Li G T, Zhang H G, Liu G D and Ma X Q 2019 *Results Phys.* **12** 1182
[35] Ruan J J, Wang C P, Yang S Y, Kainuma R and Liu X J 2014 *J. Alloys Compd.* **615** 998
[36] Hafner J 2007 *Comput. Phys. Commun.* **177** 6
[37] Perdew J P, Burke K and Ernzerhof M 1996 *Phys. Rev. Lett.* **77** 3865
[38] Perdew J P, Burke K and Ernzerhof M 1998 *Phys. Rev. Lett.* **80** 891
[39] Faleev S V, Ferrante Y, Jeong J, Samant M G, Jones B and Parkinet S P 2017 *Phys. Rev. A* **7** 034022
[40] De Freitas J M, da Veiga L M and Gonschorek W 1982 *Port. Phys.* **13** 113
[41] Zhang H G, Chen J, Liu E K, Yue M, Liu G D, Lu Q M, Wang W H and Wu G H 2019 *Intermetallics* **106** 71
[42] Liu K, Ma S C, Ma C C, Han X Q, Yu K, Yang S, Zhang Z S, Song Y, Luo X H, Chen C C and Rehman S U 2019 *J. Alloys Compd.* **790** 78
[43] Webster P J 1969 *Contemp. Phys.* **10** 559
[44] Guan Z Q, Bai J, Gu J L, Liang X Z, Liu D, Jiang X J, Huang R K, Zhang Y D, Esling C, Zhao X and Zuo L 2021 *J. Mater. Sci. Technol.* **68** 103